

# Ab initio simulation of layered amorphous graphene.

R. Thapa,\* C. Ugwumadu,† and K. Nepal‡  
Department of Physics and Astronomy,  
Nanoscale and Quantum Phenomena Institute (NQPI),  
Ohio University, Athens, Ohio 45701, USA

J. Trembly§  
Department of Mechanical Engineering  
Institute of Sustainable Energy and the Environment,  
Ohio University, Athens, Ohio 45701, USA

D. A. Drabold¶  
Department of Physics and Astronomy,  
Ohio University, Athens, Ohio 45701, USA  
(Dated: February 23, 2022)

A disorder-order transition from amorphous carbon (aC) to layered amorphous graphene (LAG) has been predicted using *ab-initio* methods. Amorphous carbon at densities close to the graphitic density show a strong proclivity to layer in NVT simulations near 3000K. Our calculations have shown that graphitization is strongly dependent on the simulation temperature and is not observed under 2500K. The origin of such a disorder-order transition has been studied using various structural analyses. Each layer of LAG is a layer of amorphous graphene (aG) including pentagons and heptagons in addition to hexagons and the planes are separated by about 3.2Å. LAG obtained from the NVT simulations were highly stable. The electronic charge density, especially for the  $\pi$  and  $\pi^*$  states, was computed with the Hyed-Scuseria-Ernzerhof (HSE) hybrid functional and compared with crystalline graphite (cG). The impact of structural disorder has been studied in detail, especially the consequences of disorder to electronic transport.

Carbon-based materials seem to have unlimited potential applications and interest [1–3], from life to Bucky Balls, and they continue to yield scientific surprises and new applications.

Graphite is an important, commonly available carbon material with many uses. A rapidly growing application for graphite is for battery electrodes in Li ion batteries [4] and is crucial for the EV industry – a Tesla model S on average needs 54 kg of graphite [5]. Such electrodes are best if made with pure carbon materials, which are becoming more difficult to obtain owing to spiraling technological demand. It is therefore of interest to determine novel paths to synthetic forms of graphite from naturally occurring carbonaceous material such as coal. This raises several questions: (1) Is it possible to convert such materials into a graphitic phase?; (2) What impurities will remain and with what technological consequences?; (3) What are the resulting properties (structural, mechanical, electrical and thermal) of such materials?

In a series of papers, we have discussed an amorphous phase of graphene, based on structural models involving pure  $sp^2$  bonding with ring disorder (that is, rather than a 2D net consisting only of hexagons, we allow for pentagons, heptagons, etc.). Among other findings, we noted that the presence of pentagons in such a structure induces puckering (de-

parture from ideal planarity) from the strain of the ring defect [6, 7]. The semi-metallic character of perfect graphene is transformed by ring disorder [8, 9].

In this Letter, we report a remarkable, disorder-order transition from 3D aC in a particular density range into aG (that is, a structure consisting of planes of aG separated by  $\sim 0.3$  nm, as in crystalline graphite). We name this Layered Amorphous Graphene (LAG). Although the transformation of crystalline  $sp^3$  bonded network of carbon (nanodiamonds, adamantane) into graphite as a function of temperature has been studied experimentally [10], there is a dearth of experiment as well as theory on its amorphous counterpart. We used standard plane wave density functional theory (DFT) simulations carrying out NVT simulations near 3000K, and show that there is a strong propensity for such systems to layer, as it is observed even for random initial configurations at suitable densities. It has long been suspected on various experimental grounds [11–13] that such a graphitization process occurs in aC, but here for the first time we demonstrate it by direct simulations and provide substantial new information about microstructure and other properties of the material. We observe that *ab initio* simulation of crystallization are rare (because the time scale for crystallization is usually very long), the best known example being extensive work on phase-change memory materials [14, 15].

In the reminder, we discuss the atomistic process of LAG formation, and explore the electronic structure, especially in the galleries (empty spaces between layers of atoms). We find there is a delocalized electron gas occupying the galleries built from bonding orbitals from the  $\pi$ -electrons. It is of technical interest that even in the presence of considerable disorder with

\* rt887917@ohio.edu  
† cu884120@ohio.edu  
‡ kn478619@ohio.edu  
§ trembly@ohio.edu  
¶ drabold@ohio.edu

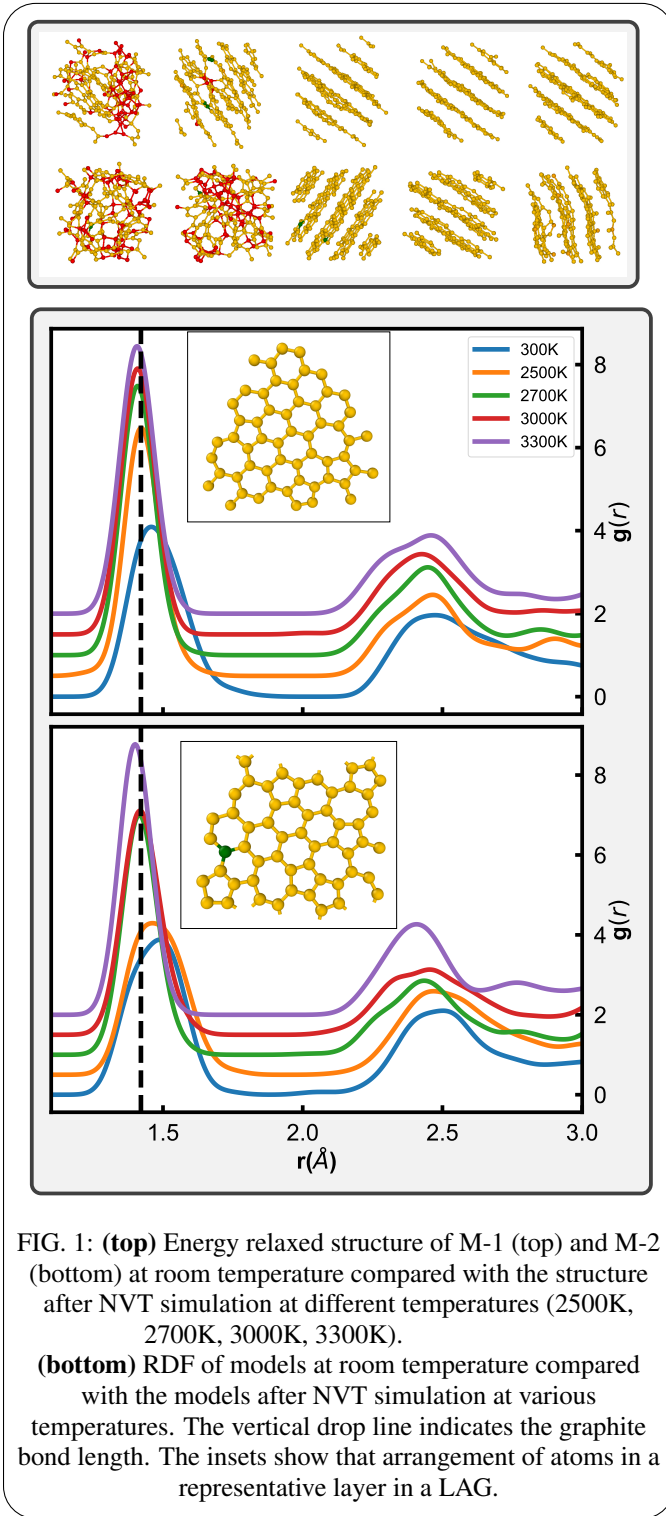


FIG. 1: **(top)** Energy relaxed structure of M-1 (top) and M-2 (bottom) at room temperature compared with the structure after NVT simulation at different temperatures (2500K, 2700K, 3000K, 3300K).

**(bottom)** RDF of models at room temperature compared with the models after NVT simulation at various temperatures. The vertical drop line indicates the graphite bond length. The insets show that arrangement of atoms in a representative layer in a LAG.

the planes that a flat layered structure forms and the origin of the binding is not van-der Waals (e.g. fluctuating dipole) interaction as often asserted, since such interactions are not included in our DFT Kohn-Sham Hamiltonian. We also discuss electronic conduction pathways in the material.

We first created a 160-atom model of aC at  $2.44\text{g}/\text{cm}^3$  with the melt-quench method [16]. The simulation was computed

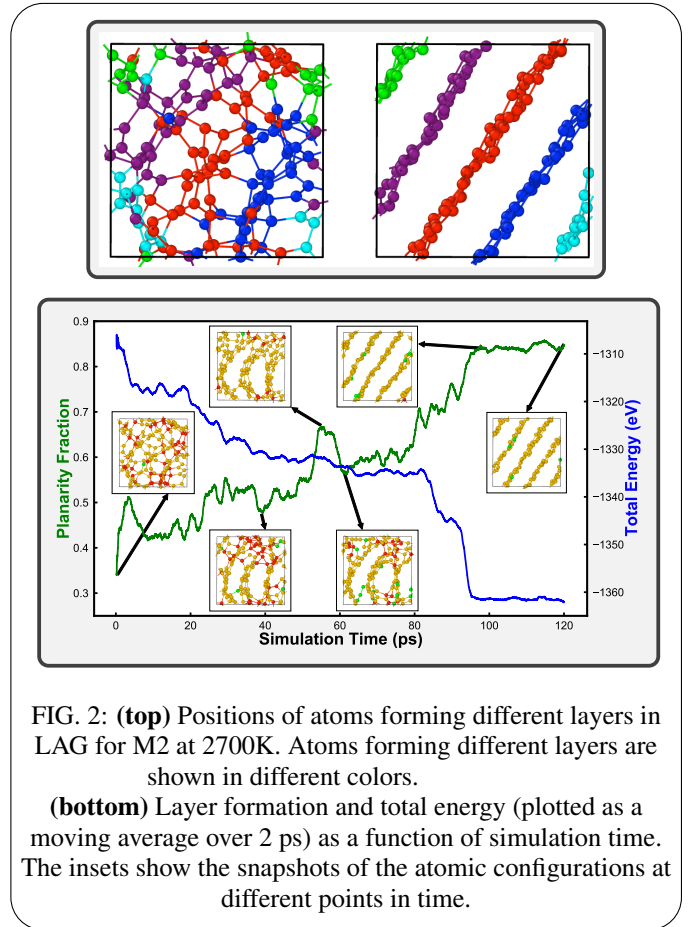


FIG. 2: **(top)** Positions of atoms forming different layers in LAG for M2 at 2700K. Atoms forming different layers are shown in different colors.

**(bottom)** Layer formation and total energy (plotted as a moving average over 2 ps) as a function of simulation time. The insets show the snapshots of the atomic configurations at different points in time.

using the Vienna *ab initio* simulation package (VASP) [17] with projector augmented wave (PAW) [18] potentials and the *Perdew-Burke-Ernzerhof* (PBE) [19] exchange-correlation functional. After the final quench was obtained, the system was relaxed. We will call this model M-1 hereafter. M-1 was subjected to NVT simulation near 3000K with the temperature being controlled using a Nose-Hoover thermostat [20, 21]. A time step of 2 fs was used and the total simulation time was kept between 100ps-120ps. The final configuration was relaxed with the forces on each atom not exceeding  $0.01\text{eV}/\text{Å}$ . For the purpose of validation and comparison of the results obtained from M-1, all the calculations were repeated on a previously published model [22] which will be called M-2. Energy for the final relaxed M-1 and M-2 LAGs were about  $0.68\text{ eV}/\text{atom}$  lower than their corresponding aC parent and about  $0.32\text{ eV}/\text{atom}$  higher than cG.

The structural transition of the aC network from disordered phase into a LAG under NVT simulation at different temperatures are shown in Fig. 1 (top). Atoms in the figures are color coded: yellow for  $\text{sp}^2$ , red for  $\text{sp}^3$  and green for  $\text{sp}$ . This color nomenclature will be used throughout unless otherwise stated. NVT simulations performed near 3000K on various sized initial configurations (20, 80, 160, 320, and 400 atoms) at  $2.44\text{g}/\text{cm}^3$  all produced LAG under simulation in VASP. The LAG formation was found to strongly depend on the density of the aC being used. Low density aC had a significant

$sp^3$  to  $sp^2$  conversion but weak layering (undulating worm-like layers) while high density aC did not layer at all owing to the limited space for the atoms to maintain a certain interplanar spacing. Layering, either flat or undulating, was observed for densities ranging between  $2.20\text{g/cm}^3$  and  $2.80\text{g/cm}^3$ . We carried out analogous simulation with an empirical potential ( Tersoff [23]) in LAMMPS [24] and did not observe LAG formation.

Since crystalline graphite (cG) is both completely  $sp^2$  and flat, we consider aC to be graphitized into LAG only if it has a significant fraction of  $sp^2$  bonding ( $> 95\%$ ) and is layered (even though not completely flat). Following this definition, we see from Fig. 1 (top) that graphitization only happens at and above 2700K in both models. However, there is a significant increase in the fraction of  $sp^2$  atoms even at 2500K. This temperature induced transition from  $sp^3$  to  $sp^2$  bonding in nanodiamond and adamantane has been studied experimentally using Raman spectroscopy [10]. In contrast to cG with a regular ordering between adjacent layers (AA, AB stacking), there is an stacking of the layers in LAG, a consequence of the presence of ring disorder. These simulations repeated on an initially random configuration produced LAG with significantly higher ring disorder. The extent of graphitization at different temperatures can be tracked with the first peak in the radial distribution function (RDF) plotted in Fig. 1 (bottom). The RDF show increased graphitic ordering as well as the ordering of the second nearest neighbor with increasing annealing temperature. The insets also show a representative layer in the LAG models with a significant fraction of ring (and bond-angle) disorder. We infer that aC to LAG transition temperature is near 2700K, provided the simulation is run for a considerable time ( $\sim 100\text{ps}$ ) with accurate interatomic interactions. The stability of LAG was confirmed by annealing at 800K and they are quite stable. A transition temperature of 3000K has been observed experimentally for production of high quality graphene using flash graphene synthesis [25].

To study the reason behind such a layering of aC under high temperature annealing, we tracked where the atoms forming the layers were located in the originally disordered structure: see Fig. 2 (top). The atoms in a particular layer of LAG are members of a connected network in the aC. The disorder-to-order transition seems describable with a nucleation theory picture with seeds of  $sp^2$  carbon growing into larger planar structures, thereby layering.

Fig. 2 (bottom) treats the time evolution of the transition. The planarity fraction is computed using the odds ratio for the likelihood of atoms forming planes. This can be thought of as a series of attempts made by the atoms to take orientations that are not only layered but also energetically favorable while maintaining some inter-layer spacing determined by the chemistry and density. The peculiar peaks around 6 ps and 57 ps suggest sharp rearrangement of atomic positions to achieve planar configurations with higher fraction of  $sp^2$  bonding. These configurations underwent additional substantial rearrangements before yielding LAG. Broadly speaking, the mechanism for the layering is to test all possible configuration within energetic constraint and the forbidden configurations which did not meet these constraints were rarely re-

peated. It is worth mentioning that after 95 ps the layering probability had reduced fluctuations as the system reached an optimized energy, as seen in the flat tail for the total energy curve (in blue).

The charge density distribution for the M2 model simulated at 2700K has been presented, together with similar calculations for cG for comparison, in Fig. 3. The charge distribution was calculated using the Heyd, Scuseria and Ernzerhof (HSE06) hybrid functional [26–28] and has been plotted along two neighboring planes of atoms (labelled ‘a’, ‘e’) and three other parallel, equally spaced slices (labelled ‘b’, ‘c’, ‘d’) in between them (in the gallery). For direct comparison, respective planes in LAG and cG have been plotted within the same color range. For plane (‘c’), the colormap shows contributions from both planes. The color maps for LAG show a more disordered distribution of charges along the planes of atoms, compared to the cG, particularly because of the presence of bond-length/bond-angle distortion, ring disorder induced puckering, etc. Our calculations have also shown that the variation of the charge density values for the LAG is higher than graphite because of the disorder. The charge distribution in the LAG galleries exhibits a low density delocalized electron gas with higher charge on the plane of atoms and monotonically decreasing as we move away into the gallery. However, we should note that the majority of the charge density on the most isolated layer from the plane of atoms (plane ‘c’ in Fig. 3 is greater than 2.0% of the maximum charge density on the plane of atoms (layer ‘a’ and ‘e’) suggesting the presence of a fairly homogeneous electron gas the galleries built from the bonding orbitals formed from the  $\pi$ -electrons.

We present in Fig. 4, information on the band decomposed charge densities for the LAG. Bands close to the Fermi level ( $E_f$ ) contain the  $\pi$  ( $E < E_f$ ) and  $\pi^*$  ( $E > E_f$ ) electrons. The  $\pi$ -bands involve much mixing from  $\pi$ -orbitals on different sites. Fig. 4a shows the  $\pi$  mixing for 3  $\pi$ -bonding orbitals, The  $\pi$ -electrons from these bands extend into the gallery creating binding between layers separated by roughly  $3.2 \text{ \AA}$ . The presence of such  $\pi$ -electrons has been reported for graphite; where it was argued that the graphene bonding forces are dominantly metallic and not van-der Waals [29, 30]. Fig. 4b shows the  $\pi^*$  anti-bonding orbitals with no charge projection to the gallery. The evidence of the electron cloud is further illustrated by projecting the charge density from the 3d box into a plane for a single  $\pi$  band and a symmetric  $\pi^*$  band in Fig. 4c and d, supporting the presence and absence of the charge density in the gallery for the  $\pi$  and  $\pi^*$  orbitals respectively.

In order to study the effects of disorder in electronic conduction and visualize the conduction active regions in the network, we calculate the space projected conductivity (SPC) [31] on LAG and compare it with that of cG. The SPC projected onto particular layers of atoms are shown in Fig.5. The SPC of an ideal graphite layer with no defects has clear paths for conduction in the plane. However, in graphite with a 5-8-5 defect, the conduction in the regions connecting the pentagons with the octagon is significantly reduced but the conductivity is still high in the regions dominated largely by hexagons. This reduction in electric conductivity in a 5-8-5 defected graphene is previously reported [32]. Similar findings were

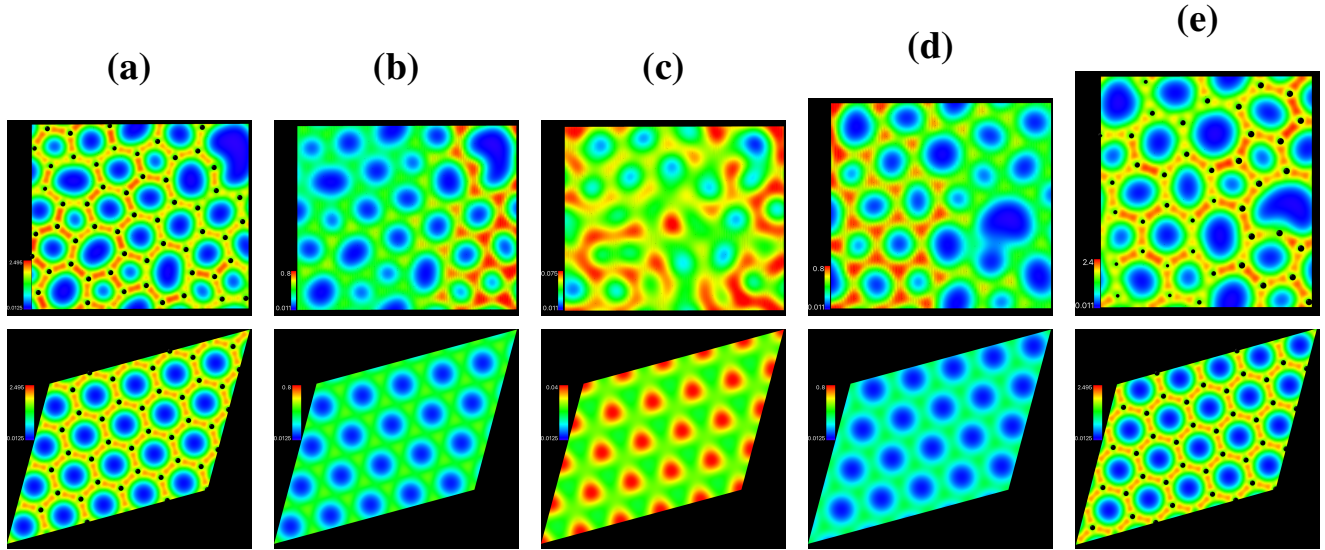


FIG. 3: **(top)** Charge density distribution on two neighboring graphitized planes for M2 model simulated at 2700K and three equally spaced slices between them. **(bottom)** Similar illustration for cG (lower panel) is included for the purpose of comparison. Black circle in (a) and (e) mark the position of the atoms in the plane.

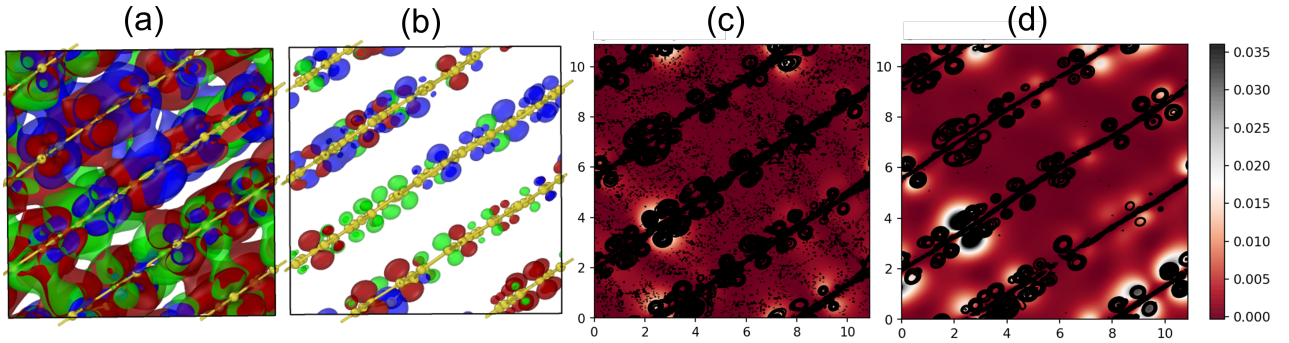


FIG. 4: Details of band decomposed charge densities for the LAG for (a) 3  $\pi$ -bands (colored blue, green, and red) in the valence region and (b) their correspondingly symmetric  $\pi^*$ -bands in the conduction region. We also show the charge density distribution for a pair of nearly-symmetric bands in (c) valence region and (d) conduction region.

seen for our atomic layers in LAG whereby the conduction paths try to avoid a junction involving a ring disorder. In other words, conduction is favored along connected atoms in hexagonal rings over non-hexagon rings. The presence of topological ring disorder significantly effects the charge transport in both graphite and LAG. We also found that the conductivity value in pure graphite is highest, followed by 5-8-5 defect graphite. The LAG conductivity was decreased by about  $10^{-2}$  relative to graphite.

In conclusion, we present evidence that LAG exists and we describe its process of formation. Plane formation is found to be robust in a suitable temperature/pressure window. LAG growth may be a practical means to obtain amorphous graphene planes in a layered graphite-like superstructure, that might even be exfoliated. We analyze the electronic structure, the mechanism of cohesion and compute the electronic consequences of ring disorder using the space projected con-

ductivity.

We thank B. Bhattacharai, E. A. Stinaff, M. E. Kordesch, M. F. Thorpe, The US Dept. of Energy for support under grant DE-FE0031981 and XSEDE (supported by National Science Foundation grant number ACI-1548562) for computational support under allocation number DMR-190008P.

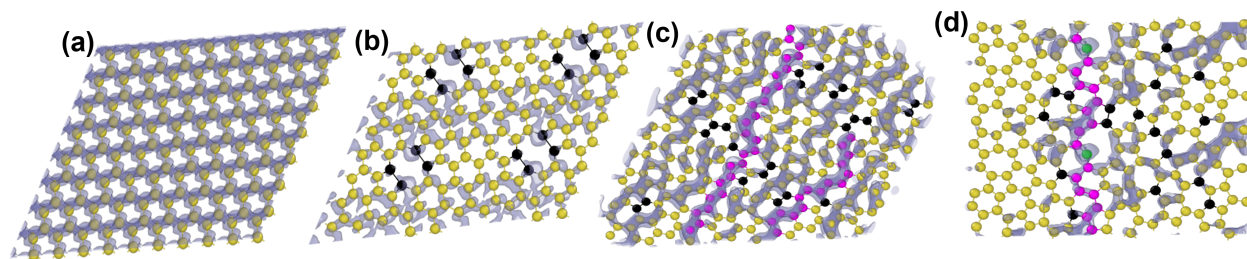


FIG. 5: SPC results (grey isosurface) for (a) an ideal graphene layer, (b) a graphene layer with 2 point defects, (c) M1, and (d) M2. Atoms in pink in (c) and (d) show atoms forming conduction path in the spatial grid, while atoms in black are border atoms where one or both neighbouring rings are non-hexagon rings. Green coloured atoms in (d) are consistent for SP atoms in M2.

- [1] C. Cha, S. R. Shin, N. Annabi, M. R. Dokmeci, and A. Khademhosseini. *ACS Nano*, 7(4):2891–2897, 2013.
- [2] R. Bafkary and S. Khoei. *RSC Adv.*, 6:82553–82565, 2016.
- [3] M. Meyyappan. *Small*, 12(16):2118–2129, 2016.
- [4] J. Asenbauer, T. Eisenmann, M. Kuenzel, A. Kazzazi, Z. Chen, and D. Bresser. *Sustainable Energy Fuels*, 4:5387–5416, 2020.
- [5] J. Desjardins. <https://www.businessinsider.com/materials-needed-to-fuel-electric-car-boom-2016-10>, 2016.
- [6] Y. Li, F. Inam, A. Kumar, M. F. Thorpe, and D. A. Drabold. *Phys. Status Solidi b*, 248:2082–2086, 2011.
- [7] Y. Li and D. A. Drabold. *Phys. Status Solidi b*, 250(5):1012–1019, 2013.
- [8] V. Kapko, D. A. Drabold, and M. F. Thorpe. *Phys. Status Solidi b*, 247(5):1197–1200, 2010.
- [9] D. V. Tuan, A. Kumar, S. Roche, F. Ortman, M. F. Thorpe, and P. Ordejon. *Phys. Rev. B*, 86:121408, 2012.
- [10] D. B. Schüpfer et al. *Carbon*, 172:214–227, 2021.
- [11] A. Barreiro et al. *Scientific Reports*, 3:1115, 2013.
- [12] B. Westenfelder et al. *Nano Letters*, 11(12):5123–5127, 2011.
- [13] T. Kim, J. Lee, and K. H. Lee. *RSC Adv.*, 6:24667–24674, 2016.
- [14] J. Hegedus and S. Elliott. *Nature materials*, 7:399–405, 2008.
- [15] J. Kalikka, J. Akola, and R. O. Jones. *Phys. Rev. B*, 94:134105, 2016.
- [16] D. A. Drabold. *Eur. Phys. J. B*, 68:1–21, 2009.
- [17] G. Kresse and J. Furthmüller. *Phys. Rev. B*, 54:11169–11186, 1996.
- [18] P. E. Blöchl. *Phys. Rev. B*, 50:17953–17979, 1994.
- [19] J. P. Perdew, K. Burke, and M. Ernzerhof. *Phys. Rev. Lett.*, 77:3865–3868, 1996.
- [20] S. Nosé. *J. Chem. Phys.*, 81(1):511–519, 1984.
- [21] W. G. Hoover. *Phys. Rev. A*, 31:1695–1697, 1985.
- [22] B. Bhattarai, A. Pandey, and D. A. Drabold. *Carbon*, 131:168–174, 2018.
- [23] J. Tersoff. *Phys. Rev. Lett.*, 61:2879–2882, 1988.
- [24] A. P. Thompson et al. *Comp. Phys. Comm.*, 271:108171, 2022.
- [25] D. Luong et al. *Nature*, 577, 2020.
- [26] J. Heyd, G. E. Scuseria, and M. Ernzerhof. *J. Chem. Phys.*, 118(18):8207–8215, 2003.
- [27] J. Heyd, G. E. Scuseria, and M. Ernzerhof. *J. Chem. Phys.*, 124(21):219906, 2006.
- [28] A. V. Krukau, O. A. Vydrov, A. F. Izmaylov, and G. E. Scuseria. *J. Chem. Phys.*, 125(22):224106, 2006.
- [29] F. Rozploch, J. Patyk, and J. Stankowski. *Acta Physica Polonica A*, 112:557–562, 2007.
- [30] E. Santos and A. Villagra. *Phys. Rev. B*, 6:3134–4141, 1972.
- [31] K. N. Subedi, K. Prasai, and D. A. Drabold. *Phys. status solidi b*, 258(9):2000438, 2021.
- [32] N. Liu, S. Zhou, and J. Zhao. *Acta Physico-Chimica Sinica*, 35(10):1142, 2019.